

# Flow and mixing near a glacier tongue: a pilot study

C. L. Stevens<sup>1</sup>, C. L. Stewart<sup>1</sup>, N. J. Robinson<sup>1,2</sup>, M. J. M. Williams<sup>1</sup>, and T. G. Haskell<sup>3</sup>

<sup>1</sup>National Institute for Water and Atmospheric Research (NIWA), Greta Point Wellington, New Zealand

<sup>2</sup>University of Otago, Dunedin, New Zealand

<sup>3</sup>Industrial Research Ltd. (IRL), Gracefield Lower Hutt, New Zealand

Received: 2 August 2010 – Published in Ocean Sci. Discuss.: 11 August 2010

Revised: 23 April 2011 – Accepted: 27 April 2011 – Published: 6 May 2011

**Abstract.** A glacier tongue floating in the coastal ocean presents a significant obstacle to the local flow and so influences oceanic mixing and transport processes. Here acoustic Doppler current profiler and shear microstructure observations very near to a glacier tongue side-wall capture flow accelerations and associated mixing. Flow speeds reached around  $40 \text{ cm s}^{-1}$ , twice that of the ambient tidal flow amplitude, and generated vertical velocity shear squared as large as  $10^{-5} \text{ s}^{-2}$ . During the time of maximum flow, turbulent energy dissipation rates reached  $10^{-5} \text{ m}^2 \text{ s}^{-3}$ , around three decades greater than local background levels. This is in keeping with estimates of the gradient Richardson Number which dropped to  $\sim 1$  during maximum flow. Associated vertical diffusivities estimated from the shear microstructure results were substantial, reflecting the influence of the glacier on velocity gradients.

## 1 Introduction

Quantifying ice-ocean interaction, especially at the small-scale, is a major challenge in high-latitude earth system sciences (e.g. Hellmer, 2004; Sirevaag et al., 2010; Rignot et al., 2010; Dimentrenko et al., 2010; Mahoney et al., 2011) where relatively long timescales and complex thermohaline and pressure effects interact with cryospheric topography that is continually changing. Oceanic mixing in polar waters includes different processes relative to those occurring at lower latitudes. For example, (i) rotational effects are large, (ii) there is little dynamic influence due to temperature, (iii) the effect of being close to the freezing temperature has a controlling influence on behaviour and (iv) there are

the additional frictional boundary effects of the frozen upper surface (McPhee, 2008).

Glacier (or ice) tongues add additional complexity to coastal ice-ocean interaction. These features, formed by glacier outflows into the coastal ocean, can extend many tens of kilometers from shore (Frezzotti, 1997) and be many hundreds of meters thick in places. Glacier tongues and ice shelves significantly influence local circulation and mixing (Jacobs et al., 1981; Legresy et al., 2004). In the case of flow past a glacier tongue, the mixing processes are then a result of the tidal and regional circulation flows past a bluff body. The closest relevant work is that concerned with flow around headlands and islands (e.g. Edwards et al., 2004), except of course with a glacier tongue the flow can pass under the obstacle as well as around.

Ice-ocean interaction processes are especially important in southern McMurdo Sound, Antarctica where Haskell Strait connects the western Ross Sea and the single cavity beneath the Ross and McMurdo Ice Shelves (Fig. 1). The Sound acts as a conduit for both ice shelf waters and warmer Ross Sea waters (Robinson et al., 2010). The fate of these waters is dependent on transport and mixing processes in the region. This exchange influences sea ice growth, which in turn affects climate processes over large space and time scales (Hellmer, 2004; Dinniman et al., 2007; Robinson et al., 2010).

The Erebus Glacier Tongue (EGT, Fig. 2) in southern McMurdo Sound has been observed to influence local vertical stratification through formation of diffusive-convective layering (Jacobs et al., 1981). It has also been suggested that such glacier/ice tongues generate local sources of supercooled water (e.g. Debenham, 1965; Jeffries and Weeks, 1992) – formed when water is cooled at depth to the in situ freezing temperature but then transported to shallower depths where it is colder than the new in situ freezing temperature. This supercooled water remains liquid until it encounters nucleation sites at which point it forms frazil/platelet ice



Correspondence to: C. L. Stevens  
(c.stevens@niwa.cri.nz)

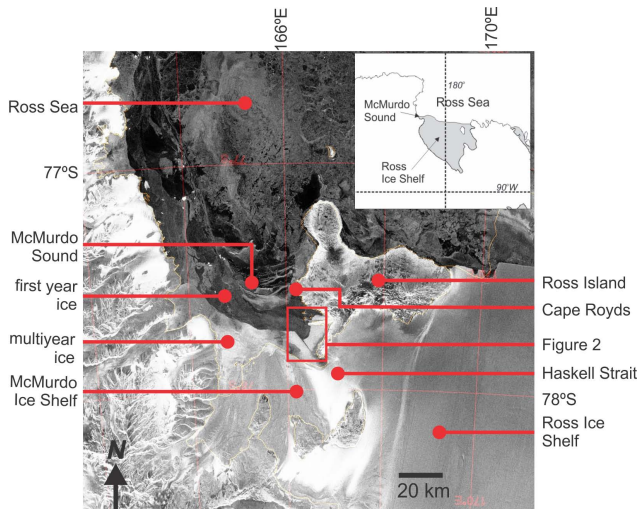


**Fig. 1.** Satellite image (SAR) captured on 19 October 2009 showing McMurdo Sound located in the south western Ross Sea connected to the Ross Ice Shelf cavity via Haskell Strait beneath the McMurdo Ice Shelf. The greyscales give an indication of open water and pack ice off Cape Royds and the first year and multiyear ice in the Sound. The inset shows the locale within the western Ross Sea.

(e.g. Dmitrenko et al., 2010). Ice crystals grow so large in McMurdo Sound (>250 mm diameter) that the largest of the frazil crystals are often referred to as platelets (e.g. Smith et al., 2001). This phenomenon is readily observed in the region (Dempsey et al., 2010) including during the very first of such measurements by Edward Nelson in 1911 during Scott's second expedition (Deacon, 1975).

The EGT site provides a system in which to examine the variability of, and interaction between, small-scale mixing and advective processes next to ice topography. Much work has examined the cryospheric mechanics and the effect of the ocean on the glacier tongue (Robinson and Haskell, 1990; Squire et al., 1994 and papers therein). Here we present new flow and turbulence measurements in order to quantify the effect of the glacier tongue on local oceanography. Whilst brief, the sampling was timed such that we captured a diurnal tidal cycle of turbulence data during the fastest tidal flows along with several tidal cycles of upper water column velocity data. These new data are potentially relevant to flow and melting processes at the face of larger glacier tongues, ice shelves and grounded icebergs (Rignot et al., 2010). The objective here is to present new shear microstructure observations providing evidence of substantial ocean mixing rates near the tip of a glacier tongue. The Discussion then explores the water column structure and kinematics, mixing, mechanisms for enhancement of local supercooling and generalization of the results beyond the EGT and how an expanded study might extend the present measurements.

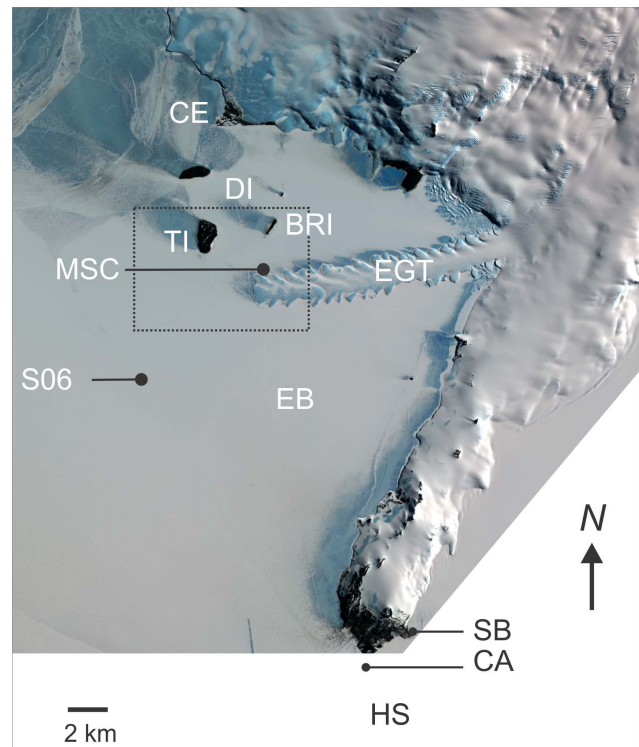


**Fig. 2.** ASTER (Advanced Spaceborne Thermal Emission and Reflection Radiometer) satellite image of south east McMurdo Sound including the Erebus glacier tongue (EGT), the Dellbridge Islands (DI) including Tent Island (TI) and Big Razorback Island (BRI), Erebus Bay (EB), Cape Evans (CE), Cape Armitage (CA), Haskell Strait (HS), Scott Base (SB) and the microstructure field camp (MSC). The measurements described in Stevens et al. (2006) come from S06. The dashed box shows the locale for Fig. 3a.

## 2 Methods

### 2.1 Location

In November 2009 we conducted exploratory oceanographic measurements within 30 m of the sidewall of the EGT at a station called Microstructure Camp (MSC). This was a pilot study for a larger experiment to follow. Tidal elevation data were recorded at Scott Base near Cape Armitage, 17 km to the south (see Fig. 2 for location) and provide a spring-neap context for the experiment.

### 2.2 Acoustic Doppler current profiler

A 300 kHz acoustic Doppler current profiler (ADCP-RDI Workhorse) was deployed at the MSC for a four day period (Fig. 4), ~1 km shoreward from the tip on the north side of the EGT (Fig. 3a). The instrument was deployed through a 650 mm diameter hole in the 2.3 m thick first year fast ice attached to the EGT. The ADCP was mounted just beneath the sea ice at a depth of 2.5 m with the first measurements starting 4 m below this. The ADCP was deployed through

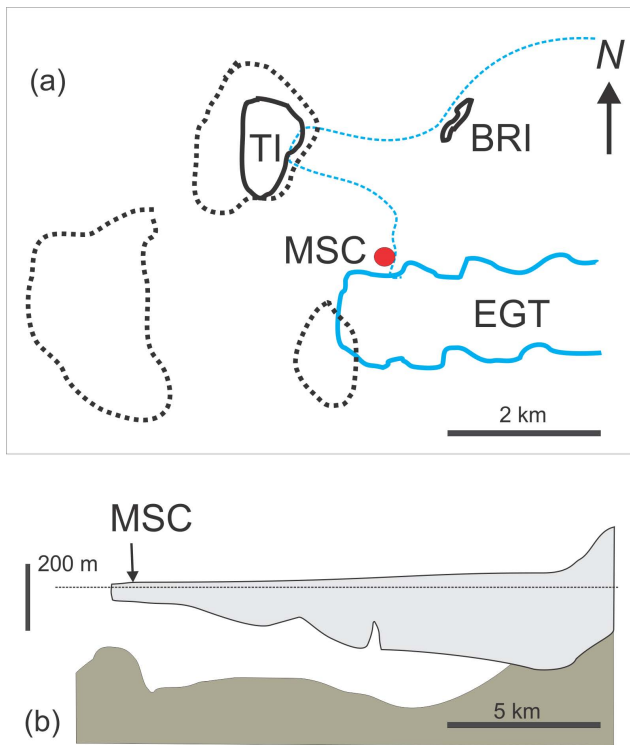


**Fig. 3.** (a) The sampling locale including the microstructure field camp (MSC), around 1000 m east of the tip of the EGT. The black dotted lines highlight the known 100 m contour whilst the blue dashed line shows a tongue of multi year fast ice (i.e. ice connected to the coast or glacier) extending out from the EGT to Big Razorback Island. (b) A cross-section of the EGT simplified from DeLisle et al. (1989).

the same hole as the microstructure profiler, with the ADCP being held to one side in a groove. We have experienced substantial interference in similar applications in other experiments. However, judicious beam orientation meant there were no obvious effects in the ADCP data due to the profiler. This was established by comparing the individual beams with one another. Also the profiler was actually only beneath the ADCP for around 50 % of the time and there was no discernable difference between the profiler being in the water vs. in the hole. The sampling recorded two-metre thick velocity bins every five minutes. Good quality data were typically resolved to depths of 70 m and as much as 120 m. This is good penetration for this type of instrument in these waters where we have previously observed far shallower penetration due to lack of suitable scatterers (Leonard et al., 2006; Stevens et al. 2006).

Velocity shear magnitude  $Sh_A$  was resolved from the ADCP vertical derivative of horizontal velocity components  $u$  and  $v$  (positive eastward and northward respectively) so that in its squared form it appears as

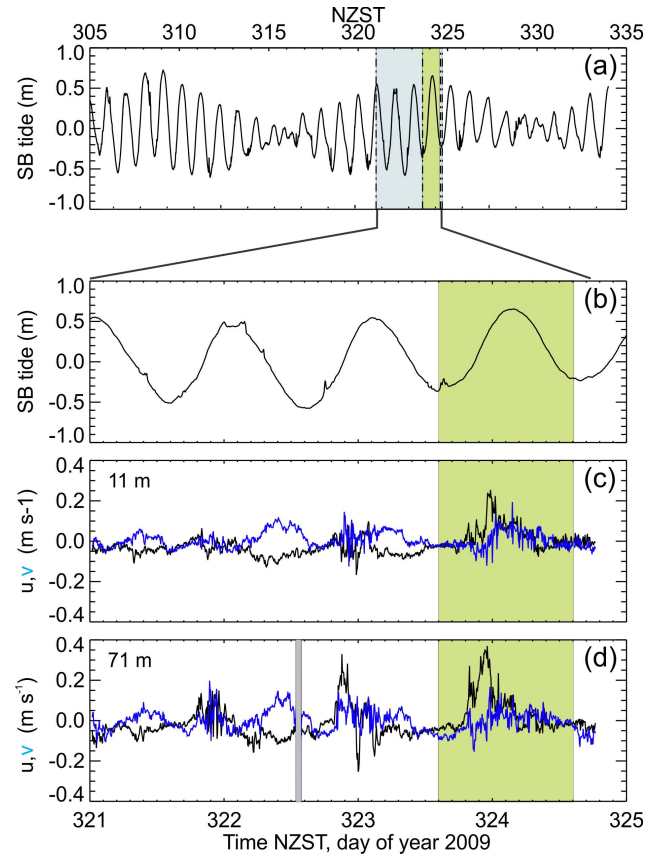


**Fig. 4.** The tidal elevation (a) at Scott Base is expanded (b) to highlight a four day segment within which our ADCP (grey box in a) and turbulence profiling (green box in all panels) were recorded. Eastward and northward currents, roughly approximating along and across glacier directions) are shown for depths of (c) 11 and (d) 71 m. The grey bar was a period of no data return from the 71 m depth range.

$$Sh_A^2 = \left( \frac{\partial u}{\partial z} \right)^2 + \left( \frac{\partial v}{\partial z} \right)^2$$

A magnetic declination offset of 144 degrees was included. Compass testing did not indicate any inconsistencies due to the near-vertical magnetic field.

### 2.3 Microstructure profiler

Turbulence properties were quantified using a Rockland VMP500 (Victoria, Canada) microstructure loose-tethered free-fall profiler with dual shear sensors (Macoun and Lueck, 2004). This enabled estimation of the turbulent energy dissipation rate  $\epsilon$  units of  $m^2 s^{-3}$  equivalent to  $W kg^{-1}$ ) his device has been used in such conditions previously (Stevens et al., 2009). The main physical modification to the profiler involved the use of a circular drag brush rather than the standard pair of square drag elements as provided by the manufacturer. This allowed the instrument to pass through

smaller holes ( $\sim 500$  mm) that possible with the square elements. Two tradeoffs were that (i) there was more vibration than with the square brushes and (ii) that the round brushes promoted rotation (as many as 10 full rotations in 250 m) during profiling that was not completely reversed on recovery. This latter effect began to seriously affect the cable integrity until we took action to counter the rotation by reversing the brushes, as well as leaving the profiler to freely spin at the end of each profile.

As described in Stevens et al. (2009), energy dissipation rates were resolved from the dual shear probe profiler using standard techniques (Prandke, 2005). The profiles were segmented into 5 m thick bins that were overlapped by 50%. Analysis first corrected for profiler vibration, then identified the reliable section of the spectrum by comparing with the vibration spectrum derived from accelerometers – generally over a range from 1 to 30 cycles per meter. The tail beyond this vibration limit was substituted with the tail of a Nasmyth model spectrum (Roget et al., 2006). The dissipation rate was then calculated with the integral

$$\varepsilon = 7.5\nu \int_k S_m dk$$

(Prandke, 2005; Wolk et al., 2002) where  $k$  is the wave number and  $S_m$  is the shear spectrum. The noise floor in terms of  $\varepsilon$  was around  $3 \times 10^{-10} \text{ m}^2 \text{ s}^{-3}$ . This was, however, not a fixed quantity as it depended on a number of variables like cable influence that were not exactly the same in every profile. Thirty eight profiles were recorded, with a total profiled distance of over 11 km.

While the profiles penetrated to  $\sim 300$  m depth, only the upper 120 m are considered here in order to focus on the influence of the glacier. Due to operational constraints there were a number of gaps in the profiling, most notably a 2.5 h gap. Fortunately, from the perspective of identifying dominant events, this gap fell during a period of slower flow.

## 2.4 Conductivity, temperature depth measurements

Conductivity-temperature-depth (CTD) profiles were acquired using a Seabird Electronics (SBE, USA) temperature (SBE 3) and conductivity (SBE 4) sensor pair mounted on the VMP500. These sensors were un-pumped so as to not affect the shear data through the creation of vibration, so the spatial resolution was  $\sim 1$  m. The profiler was kept in the water continuously so that the entire package remained at the ambient temperature removing thermal inertia start-up effects. The buoyancy frequency squared was calculated from the vertical derivative of potential density  $\partial\sigma_\theta/\partial z$  so that

$$N^2 = \frac{g}{\rho_0} \frac{\partial\sigma_\theta}{\partial z}$$

where  $\rho_0$  is a reference (background) density and  $g$  is gravitational acceleration. The gradient Richardson Number compares buoyancy and shear so that,

$$Ri_{gr} = \frac{N^2}{Sh_A^2}$$

provides a measure of shear-induced instability whereby values substantially less than unity are likely to be or become unstable. Values of  $Ri_{gr}$  where  $N^2$  was less than  $10^{-8} \text{ s}^{-2}$  were rejected (around 8% of data values) as being the noise floor of the calculation.

CTD data recorded in the vicinity of the EGT in previous seasons (4 and 5 November 2005, 11 and 13 November 2008 and 16 November 2009) by the authors provides a useful context. Profiles were recorded using a SBE 19+ CTD that was calibrated prior to, and after, the experiments.

## 3 Observations

### 3.1 Sea-ice conditions, regional circulation and tides

The tip of the EGT extends a few km beyond the multi-year ice in Erebus Bay, and is surrounded by first-year fast ice about 2.3 m thick. At the time of sampling McMurdo Sound sea ice cover was in retreat after a decade of record coverage due to the large icebergs of the early 2000's (Robinson et al., 2010). Pack ice and open water were present off Cape Royds some 20 km to the north of the sampling location. Much of the Sound from this line, down to a little south of the EGT was first year ice (Fig. 1) with multiyear fast ice confined to the western shores and Erebus Bay. The tip of the EGT extends into 2.3 m thick first year fast ice beyond the fast ice by a few km and there was no open water or pack ice until at least 10 km north of the field site. There was a residual multiyear ice bridge of ice at least 4 m thick running between the EGT and Big Razorback Island (Fig. 3).

Available data on near-surface residual circulation are sparse but suggest a predominant northward current near the south of Erebus Bay (Fig. 2), at least during winter (Leonard et al., 2006; Mahoney et al., 2011). The primarily diurnal tides in the region are around 1 m in peak-peak elevation (Goring and Pyne, 2003) with a  $\sim 14$  day spring-neap cycle (Fig. 4a and b). Tidal flows some 5 km to the SW of the EGT (Site S06 on Fig. 2) reached maximal amplitudes of  $\sim 0.20 \text{ m s}^{-1}$  (Stevens et al., 2006) and residuals of  $0.05 \text{ m s}^{-1}$ .

### 3.2 Velocity data

While the tides typically generate maximum flows of  $\sim 0.15$ – $0.20 \text{ m s}^{-1}$  in the Sound-proper (Barry and Dayton, 1988; Leonard et al., 2006; Stevens et al., 2006), at the MSC station we saw flow magnitudes reach  $0.40 \text{ m s}^{-1}$  (Fig. 4c and d). The currents appear moderately cyclical (Fig. 4c and d)

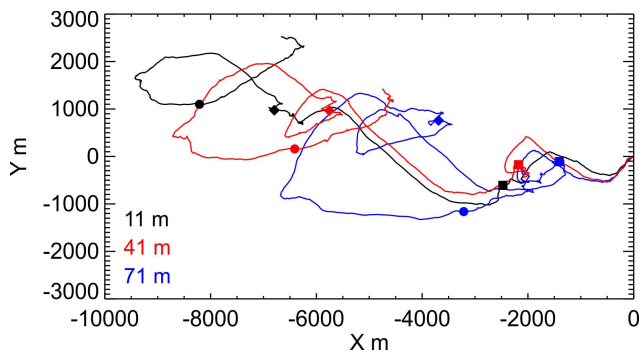


**Fig. 5.** Horizontal velocity data as a progressive vector diagram showing 11 (black), 41 (red) and 71 (blue) m depths. The start of each day is marked with a symbol (square = 322, diamond = 323 and circle = 324 NZST).

but careful examination reveals the faster flows in each cycle were not phase-locked to the tide. The short duration of the dataset precluded any co-spectral analysis. The faster flows occurred on the rising/high tide and were variable in magnitude and direction. The strongest flow was quite short in duration in each tidal period and so we refer to it here as a pulse, in an otherwise moderately quiescent water column.

A progressive vector diagram (Fig. 5) that separated near-surface (black), EGT base (red) and deeper (blue) flows shows that there was a consistent weak westward flow towards the EGT tip but that there were some clear differences in apparent trajectory. Around day 323 the intermediate and deeper flows reversed whilst the shallower flow did not, reflecting a baroclinic effect resulting in tidal rectification. This diagram shows the westward trend towards and to the north of the EGT tip clearly along with the anti-clockwise sense of the rotation.

Focusing on the period when there were concurrent microstructure and CTD data (323.6–324.6) enables closer examination of the pulse which was the strongest measured flow during the sampled period (Fig. 6). During this day the pulse was located on the rising phase of the tide (323.85–324.05) moving largely eastward and, at the observation point at least, this was seen as flow acceleration initially at depths below 40 m (Fig. 6) at which time flows shallower than this were towards the EGT. The pulse then expanded to fill the entire measured depth before decaying. The main body of the pulse (P in Fig. 6) lasted  $\sim 4$  h. It was followed by apparent oscillations or waves (W in Fig. 6) whereby there were moderate flow accelerations for short periods spaced  $\sim 70$  min apart. Directionally, the flow within the pulse was directed to the north-east whilst the flow before and after varied but with a net westerly direction towards the tip. Flow magnitudes other than during the pulse were comparable with measurements made elsewhere in the Sound at locations further away from the coast or glacier walls (Stevens et al., 2006; Robinson, 2011).

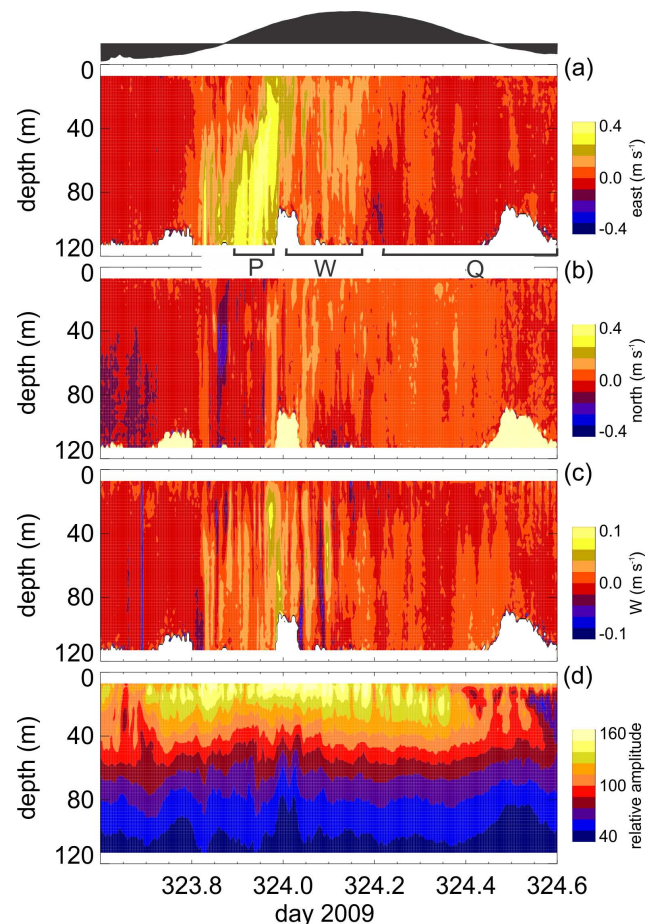


**Fig. 6.** ADCP data products. The ADCP resolved (a) eastward velocity, (b) northward velocity, (c) upward velocity  $w$ , and (d) backscatter amplitude as a function of time (NZST = UTC+12). The approximate local depth range of the glacier is shown as horizontal dashed lines. The tidal elevation is shown not to scale above panel (a). The blank sections at the base of panels (a), (b) and (c) are where there was insufficient backscatter to calculate good quality velocities. The pulse (P), waves (W) and quiescent (Q) periods are marked above (b).

The flow pattern included strong vertical flows that reached up to  $10 \text{ cm s}^{-1}$  (Fig. 6c). The main body of the pulse was preceded by an initial downwards flow, largely upwards flow during the pulse, and finally with a strong increase in speed at the cessation of the pulse. The vertical flows were reduced in magnitude near the surface. The post-pulse oscillations were seen in both vertical and horizontal velocities. Furthermore, as the post-pulse oscillations had a half-period timescale of 35 min and a vertical speed of  $\sim 0.05 \text{ m s}^{-1}$  then the individual events might be expected to advect water  $\sim 100$  m vertically in this time.

Backscatter amplitude variations as seen here (Fig. 6d) often provide a qualitative picture of a tracer field (Leonard et al., 2006; Stevens et al., 2006). It is a difficult property to

interpret as it is an integral whereby the value at a given depth is a function of the water column through which the acoustic beams must pass twice. Hence, a low acoustic backscatter at say 80 m might indicate few reflectors at that depth or a high degree of acoustic attenuation above the sample volume. There were three periods in the 24 h when the backscatter was reduced enough to affect the velocity signal to noise ratio adversely, reducing the deepest depth of good quality data. These reductions were pre- and post-pulse, as well as a sustained quiescent period occurring 12 h after the pulse (Q in Fig. 6). This might be a diurnal cycle in scattering due to biological modulation as, despite the 24 h daylight, a variation in signal can persist in the region (personal communication A. Mahoney; Leonard et al., 2010) or due to variations in platelet/frazil ice concentration (Stevens et al., 2006). Our sampling coincided with a period when the pulse occurred near midnight local time ( $\sim 11:00$  UTC) so it was co-located temporally with what should be a biologically-induced maximum data return (i.e. good signal to noise). Furthermore, this diurnal variation was not nearly as strongly apparent on other days. Thus, the drop in backscatter may have instead been a response to the stronger flow. Curiously, at the end of the data shown in Fig. 6d there was a period when there was a local minimum in backscatter between 20 and 40 m depth. This effect was not seen in earlier measured tidal periods when the flow was weaker.

### 3.3 Temperature and salinity

A diurnal cycle of CTD data revealed the very small thermal (8 mK) and salinity (0.04 PSU) ranges (Fig. 7). The potential temperature and salinity fields remained quite constant except for a cool/fresh flow before and after the pulse which itself was warmer and fresher than background levels. The net dynamic result (Fig. 7d) was a decrease in potential density just prior to the pulse when the local fluid was heavier than background levels. The trailing oscillations were then lighter, especially near the surface. The remainder of the diurnal period slowly increased in potential density with a lighter surface layer. The temperatures were well above the in situ freezing point and so there was no supercooling (Fig. 7b).

### 3.4 Stability and turbulence

ADCP velocity shear magnitude squared  $Sh_A^2$  was typically in the order of  $3 \times 10^{-7} \text{ s}^{-2}$ , although during the main pulse flow it reached six times this value i.e.  $9 \times 10^{-6} \text{ s}^{-2}$  (Fig. 8a). At the same time, the stratification persisted during the strongest section of the pulse flow as the  $N^2$  was greatest during and just after the flow pulse (Fig. 8b) when fresher and lighter fluid appeared in the upper 40 m of the water column and  $N^2$  reached  $10^{-5} \text{ s}^{-2}$ . During the period of post-pulse oscillation  $N^2$  was at detectable limits of  $\sim 10^{-8} \text{ s}^{-2}$ . These values bracket other comparable observations in the

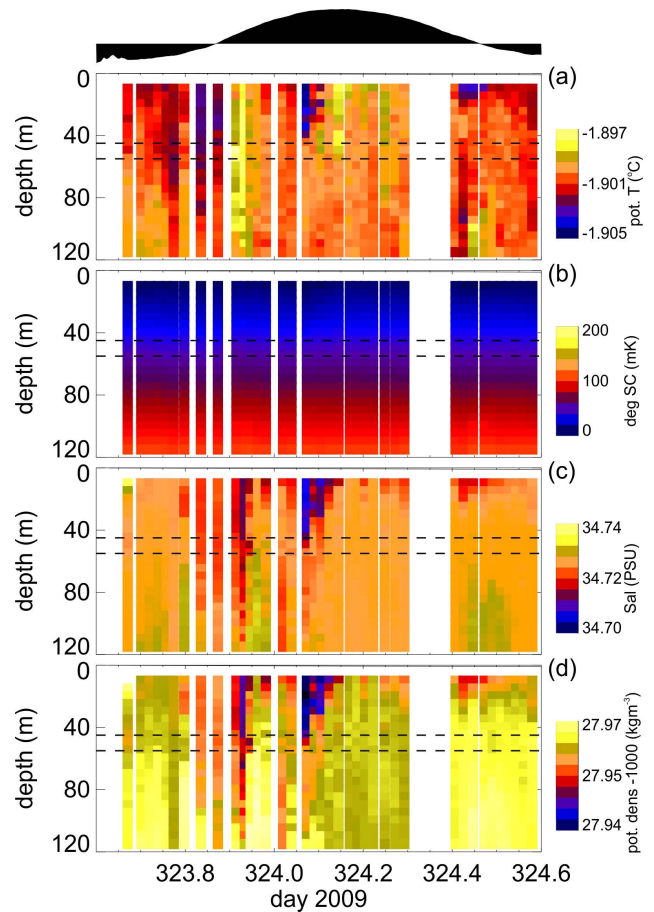


**Fig. 7.** CTD scalar data products as a function of time (NZST = UTC+12) showing (a) potential temperature, (b) degree of supercooling (in situ temperature–local freezing temperature), (c) salinity and (d) potential density anomaly. The approximate local depth range of the glacier is shown as horizontal dashed lines. The tidal elevation is shown not to scale above panel (a).

Sound where  $N^2=3 \times 10^{-6} \text{ s}^{-2}$  was observed over the ridge running off Cape Armitage (Stevens et al., 2009).

The turbulent energy dissipation rate  $\varepsilon$  reached a maximum of  $10^{-5} \text{ m}^2 \text{ s}^{-3}$  (Fig. 8c). Such high dissipation rates were mostly confined to the upper 40 m of the measured water column for a period of  $\sim 4$  h. The post-pulse oscillations were aliased in the profiling so that any elevated  $\varepsilon$  events associated with these brief accelerations were not necessarily captured. After the post-pulse oscillations finished,  $\varepsilon$  dropped to  $\sim 10^{-7} \text{ m}^2 \text{ s}^{-3}$  and then, after the final backscatter minimum (time 324.5; midday 21 November 2009), it fell, at least at depths greater than the thickness of the EGT, to the noise floor of the instrument. The  $\varepsilon$  is compared with the  $Ri_{gr}$  (Fig. 8d) in Sect. 4.2.

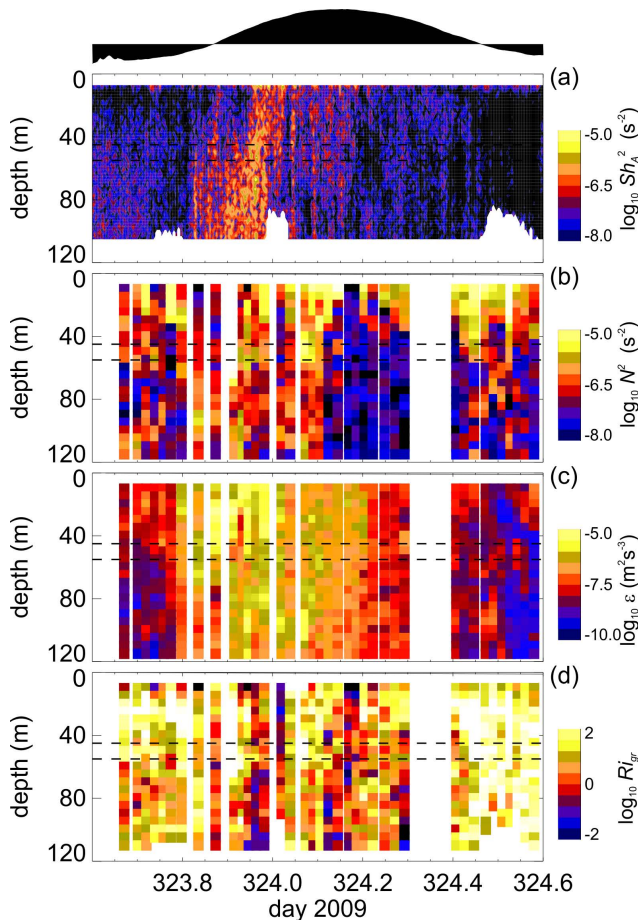


**Fig. 8.** Calculated properties including (a) ADCP-resolved shear  $Sh_A^2$  and VMP profiler-resolved (b) buoyancy frequency squared  $N^2$ , (c) turbulent energy dissipation rate  $e$  and (d) the  $Ri_{gr}$  as a function of time (NZST = UTC+12). The approximate local depth range of the glacier is shown as horizontal dashed lines. The tidal elevation is shown not to scale above panel (a). The blank sections at the base of panels (a) and (d) are where there was insufficient backscatter to calculate good quality velocities.

## 4 Discussion

### 4.1 Kinematics and water column structure

The observations reported here were obtained at a time of extremely weak stratification. Of the three field seasons we have worked in the area, these conditions were the most weakly stratified (Fig. 9). Indeed even CTD profiles a week prior to the present data indicated substantially stronger stratification. Furthermore, the profiles from 2009 (red and black in Fig. 9) were also the warmest and saltiest observed at this location. Wintertime results from a site several km to the south of the present field site in Erebus Bay showed how fronts passed through the observation site changing the local density structure markedly in only a few hours (Mahoney et al., 2011). These data end a month prior to our measurements

and at the end of their record their temperatures were around  $0.02^\circ\text{C}$  colder than our observations – more in keeping with previous CTD work (Fig. 9). Consideration of variations in water mass suggest that McMurdo Sound was still adjusting and recovering from the large iceberg residences of 2002–2005 (Robinson, 2011). The wider Sound water mass data showed a general trend of increasing salinity largely commensurate with that captured here. Furthermore we speculate that the T and S variation seen closely tied to the flow might be a direct manifestation of the flow-glacier interaction. Cold fresh water might pool in the vicinity of the EGT due to flow blocking and then be washed away during the pulse.

Flow at the field site was likely a combination of tidal and residual flows that are affected by the islands, local bathymetry and the glacier tongue itself. There is unlikely to be direct wind influence as open water was 20 km to the north. The net flow was weakly to the north-west with the fastest flows (albeit for brief periods) in a north easterly direction (i.e. away from the tip). Residual flows on the east side of the Sound have mostly been southward (Barry and Dayton, 1988; Dinniman et al., 2007; Robinson, 2011) although some authors suggest northward flow is possible (Lewis and Perkin, 1985). This suggests our observations show the influence of tidal rectification whereby the close presence of topography results in the tide being asymmetric. Consequently our results could be influenced by the combined effects of the EGT and Tent Island to the north rather than the EGT alone.

The local maximum thickness of the EGT ( $\sim 50\text{--}60\text{ m}$ ) did not readily reveal itself in any of the profile data. One might reasonably have expected a step in stratification or a strongly consistent velocity shear feature. That neither of these were apparent is indicative of the fact that the underside of the glacier tongue is not level either along, or across, its main longitudinal axis (Holdsworth, 1982). The effect of the sloping convex underside of the glacier tongue will be to distribute the depth of the glacier-generated flow and associated mixing and so making it hard to identify in scalar profiles.

In the case of the near-EGT flow, the response of the flow will manifest itself in a manner depending on the stratification. In the present situation the post-pulse oscillations were comprised of accelerations  $\sim 70\text{ min}$  apart. There are a range of relevant frequencies to consider (Albrecht et al., 2006). Here  $N^2$  varied from  $10^{-8}$  to  $10^{-5}\text{ s}^{-2}$  implying timescales of 17 h and 33 min respectively so it does cover the observed 70 min period. Consideration of vertical velocity spectra both near the surface and deeper (Fig. 10) shows the deeper water exhibiting greater periodic energy at frequencies  $< 20\text{ cpd}$  (i.e.  $> 72\text{ min}$ ). The standard deviation of vertical velocity at the three depths plotted in (Fig. 10) were 9, 15 and  $16\text{ mm s}^{-1}$  at 12, 40 and 60 m depths respectively. This suggests there was greater energy being transferred through the internal wave spectrum in the water column beneath the tongue. This is sensible as (i) vertical flows will attenuate to zero at horizontal surfaces, (ii) the fast ice-driven boundary

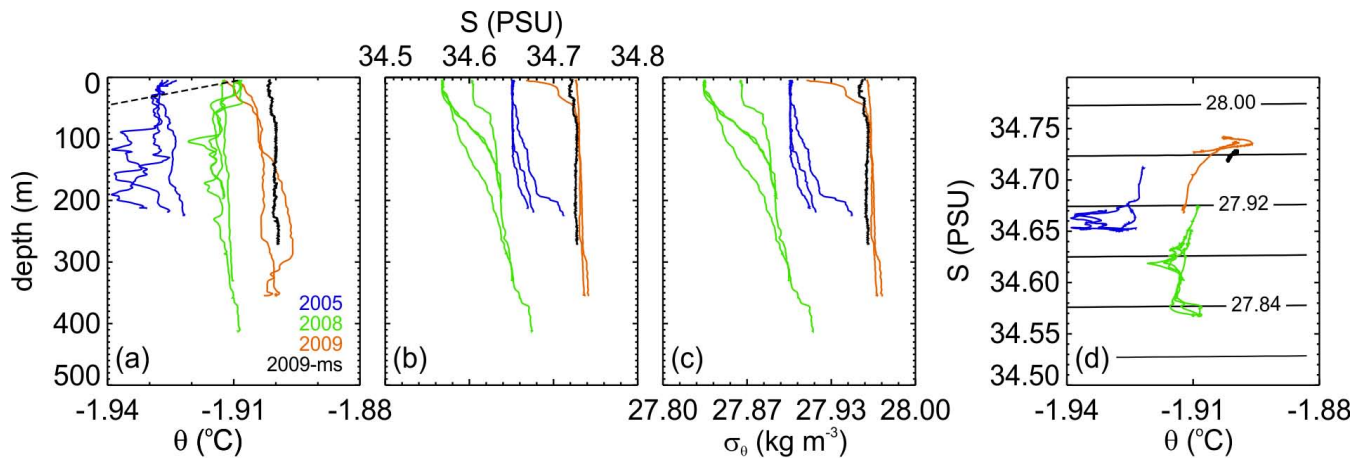


**Fig. 9.** (a) Potential temperature, (b) salinity, (c) potential density anomaly profiles at various locations within 500 m of the tip of the EGT from the October–November period during 2005, 2008 and 2009, plus a single representative example from the present microstructure data (2009 ms). The dashed line in the upper part of (a) is the freezing temperature at a nominal salinity of 34.65 PSU. The maximum depth from the 2005 profiles were limited by operational issues. The other CTD profiles all penetrated to within 20 m of the bed indicating the large variation in depth in the region. (d) Shows the  $-S$  relationship superimposed onto potential density anomaly lines.

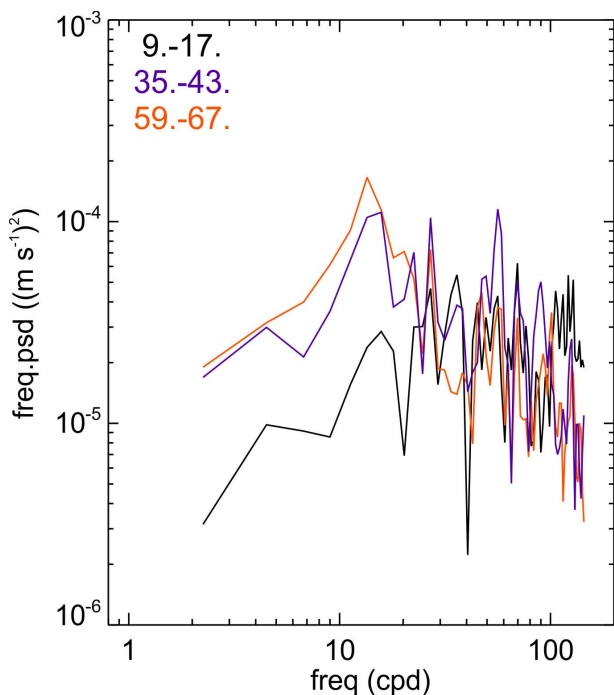


**Fig. 10.** Spectra of ADCP-derived vertical velocities from depths 9–17, 35–43 m and 59–67 m. The timeseries were 72 h long and the spectra are shown scaled by the frequency vector to provide an area-preserving form.

layer is unable to support internal waves and (iii) internal waves persist at depths other than that at which the obstacle exists (e.g. mountain lee waves).

The Strouhal number  $St = fL/u$  ( $f$  is shedding frequency,  $L$  is a body lengthscale either vertical or horizontal, and  $u$  is velocity) is in the range 0.03–0.3 (assuming  $f = 2 \times 10^{-4} \text{ s}^{-1}$ ,  $L = 50\text{--}500 \text{ m}$  and  $u = 0.3 \text{ m s}^{-1}$ ). This intermediate flow regime suggests variable flow with buildup and release of vortices (Sobey, 1982). Thus, on the inward flood tide into the Dellbridge Islands embayment, vortices are possibly shed off the tip of the EGT. On the return tide the decaying waves are advected away from the EGT. While progressive vector diagrams like Fig. 5 should be interpreted with care it does illustrate the distances material might move in a few tidal cycles.

Not only does melting of glacier and ice shelf walls have a strong influence on ice dynamics (Rignot et al., 2010; Olbers and Hellmer, 2010), it can also result in highly variable stratification near the wall, including double diffusive layering (Jacobs et al., 1981). Whilst the present study was initially motivated by the search for diffusive convection as observed in the Jacobs study, we didn't observe the correct conditions for this process and so were unable to compare the magnitudes of shear-induced and double diffusion-induced turbulent mixing. It seems highly likely that the pulse feature would sweep away layering structure generated by double diffusion. However, the pulse is transient and so for the majority of the time conditions were relatively quiescent (Q in Fig. 6) and thus conducive to the accumulation of melt water. Hence, further exploration of the melting processes needs to incorporate temporal variation in the ambient conditions at timescales less than a tidal period.

### 4.2 Mixing rates

The energy dissipation rate ( $\varepsilon$ ) rose, albeit for localized moments in time, as much as three orders of magnitude above what might be regarded as normal background levels ( $\sim 10^{-8} \text{ m}^2 \text{ s}^{-3}$ , Stevens et al., 2009). In a situation with similar headland scale and flow speeds Edwards et al. (2004) quantified how local turbulent buoyancy flux scaled with  $\varepsilon$  and that it is likely maximum very close to a headland. Recent modeling efforts (Dinniman et al., 2007; Reddy et al., 2010) that encompassed the region were at scales ( $>5 \text{ km}$ ) that are unlikely to be instantaneously influenced even by this degree of variability. Evidence from elsewhere suggests such sub-grid scale mixing processes can be influential at the scale of the Sound (e.g. Xing and Davies, 2010).

Modelling typically parameterizes internal energy dissipation and diffusion as a function of  $Ri_{gr}$ . Typically this is highly variable, being the ratio of two derivative properties, so that noise and uncertainty are substantial. However, the depth-time distribution of  $Ri_{gr}$  does have some consistent structure (Fig. 8d) in the core of the pulse  $Ri_{gr} < 1$ , implying mixing due to shear is likely and this was consistent with the dissipation rate observations. At times away from the pulse feature, stratification persisted more strongly so that  $N^2 = 10^{-5} \text{ s}^{-2}$  and background shear was more like  $Sh_A^2 = 3 \times 10^{-8} \text{ s}^{-2}$ . Under these conditions  $Ri_{gr} \sim 300$ , implying local shear-induced mixing was unlikely.

There are trends between the estimate of the  $Ri_{gr}$  and the measured dissipation and inferred vertical diffusivity  $K_\rho$  (Fig. 11). We estimate  $K_\rho$  using the model proposed by Shih et al. (2005) for energetic growing turbulence, likely at least during the pulse,

$$K_\rho = 2\nu \left( \frac{\langle \varepsilon \rangle}{\nu \langle N^2 \rangle} \right)^{1/2}$$

where  $\langle \rangle$  denotes ensemble averages. We also compare these values with the estimates of Fer (2006) who suggests modification of the background levels in the Pacanowski and Philander (1981) formulations for vertical eddy viscosity (of momentum,  $K_m$ ) and vertical eddy diffusivity (of buoyancy,  $K_\rho$ ). The modifications were based on observations in an Arctic fjord and so arguably more relevant here due to the proximity to topographic variations than an open ocean parameterization. The Fer (2006) parameterizations are given as

$$K_m = \frac{5.5 \times 10^{-3}}{(1 + 5Ri_{gr})^2} + K_{m0} \quad (1)$$

$$K_\rho = \frac{K_m}{(1 + 5Ri_{gr})} + K_{\rho0} \quad (2)$$

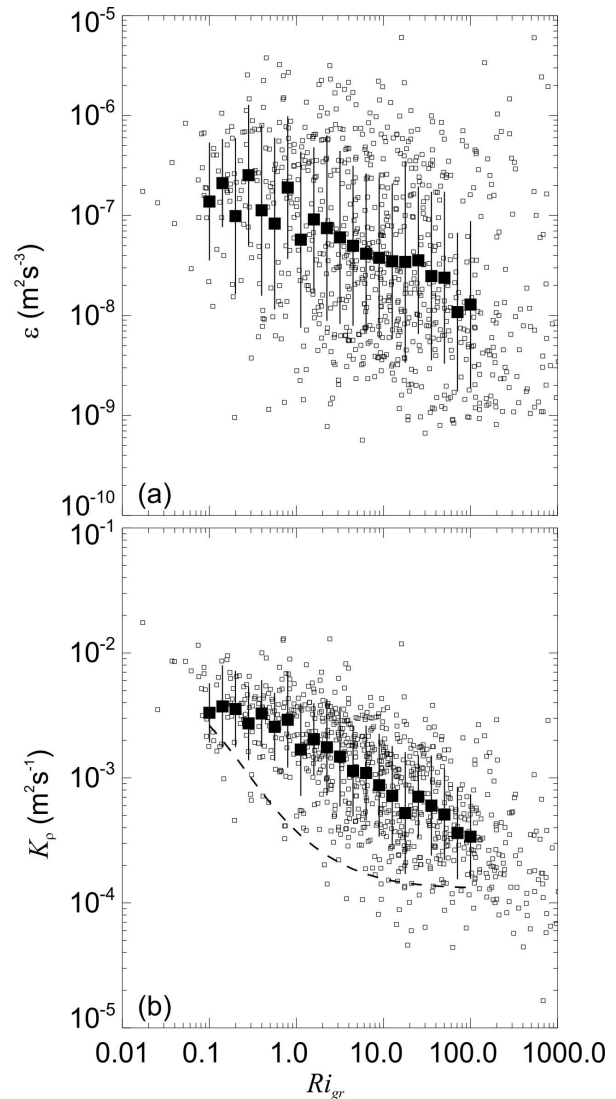


**Fig. 11.** (a) Dissipation rate as a function of  $Ri_{gr}$  showing individual estimates (hollow squares), bin-log-space-averaged (solid squares) and bars showing standard deviation of estimates for 0.15  $\log(Ri_{gr})$  spaced bins. (b) The Shih et al. (2005) estimate of diffusivity  $K_\rho$  and the Fer (2006) parameterization of vertical diffusivity of mass (dashed line).

where background levels are given by  $K_{m0} = 1.3 \times 10^{-3} \text{ m}^2 \text{ s}^{-1}$  and  $K_{\rho0} = 1.3 \times 10^{-4} \text{ m}^2 \text{ s}^{-1}$ . Here the Shih et al. (2005) diffusivity is larger than the model determined by Fer (2006) – especially in the  $Ri_{gr} = 1-10$  band.

The Fer (2006) model uses the Osborn method to determine (1) and (2) which it notes is an upper bound (Osborn, 1980; Zaron and Moum, 2009). The difference potentially lies in the small spatial scales of variability as the observed  $N^2$  may not be particularly representative of the conditions that spawned the mixing. As we have no direct measure of  $K_\rho$  it is important to note we are not suggesting present

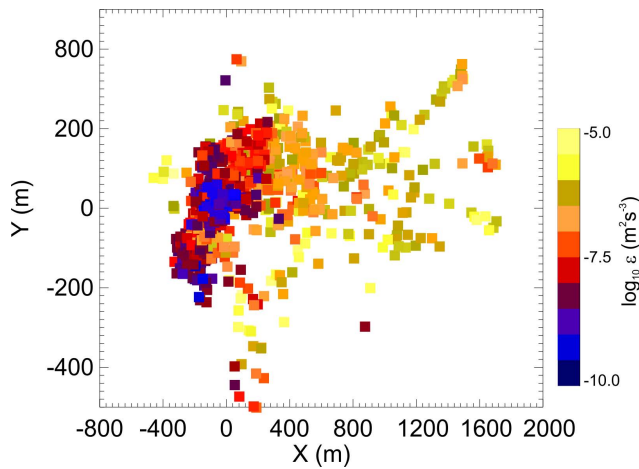


**Fig. 12.** All dissipation rate estimates over the 24 h sampling period as a function of pseudo “horizontal displacements” X and Y using a timescale of 35 min.

parameterization (Fer, 2006) is generally incorrect but rather that it may not be applicable so close to ice walls.

It is useful to consider the relationship between displacement and energy dissipation. Assuming a timescale of  $\sim 35$  min associated with the half-period of the oscillations (i.e. the period motion will be in a particular direction and so giving the maximum excursion) it is possible to place the dissipation rate estimates on a displacement diagram (Fig. 12). It is clear that the eastward flowing periods generated the strongest dissipation rates and the displacements were comparable with the distance to the tip of the glacier tongue. Thus, the observations downstream might potentially be the result of direct flow-obstacle interaction. There are strong similarities between the velocities, diffusivity and dissipation rates observed here and by Edwards et al. (2004). Finescale modeling might elucidate the distribution and longevity of such mixing regions.

### 4.3 Local supercooling

A number of authors have suggested that glacier/ice tongues might be generators of supercooled water (Debenham, 1965; Jeffries and Weeks, 1992). Such conditions arise because seawater in contact with ice at depth is cooled to the in situ freezing point, but at some later time if it rises in the water column, the increase in local freezing temperature (due to pressure decrease) results in the fluid actually being colder than this freezing temperature. This substantially increases its propensity to freeze. While this is unlikely in the particular relatively warm period observed here, there have been previous times even at the same time of year when it does occur as shown in the CTD data in Fig. 9. Thus, the presently observed kinematics are relevant to the supercooling problem. The ADCP data do show a weak upward flow for most of the time. Earlier it was demonstrated that the post-pulse

oscillations might be expected to advect water  $\sim 100$  m vertically. This displacement represents a  $-0.075$  °C change in the in situ freezing point; thus, if the rising water is very cold to begin with there is a strong possibility it will form platelets.

Platelet growth rates are very difficult to quantify as they inherently depend on their initial conditions and observations have difficulty in separating advection versus actual growth. However, Leonard et al. (2006) observed cylinders of platelets 30 cm in diameter growing on near-surface mooring lines after periods as short as three days. This suggests that if, as the observations suggest (Fig. 5), the flow were rectified in some way then platelet growth might ensue. Similar possibilities exist due to the internal waves observed at Cape Armitage 17 km to the south of the EGT (Robinson, 2011). Thus, these highly localized features could potentially act as “ice factories”.

## 5 Generalization, conclusions and future work

Clearly the glacier forms a substantial obstacle that causes blocking and local mixing. Furthermore, sharp headlands strongly influence local flow through rectification of tides (e.g. Signell and Geyer, 1991; Edwards et al. 2004). Although the EGT’s elongated morphology is at the extreme end of the headland aspect ratio scale and glacier tongues are located at the surface rather than the bed, we expect there is much in common in terms of oceanic response to tidal flow. The headland work of Edwards et al. (2004) identified the split between skin and form drag and that the majority of the diapycnal turbulent buoyancy flux occurred close by the headland. This supports the contention that more turbulence data very close to the glacier wall would help to identify the dynamic importance of such features.

The EGT has quite a large aspect ratio (length/width) when compared to the Drygalski Ice Tongue (and the Mertz and Ninnis Glacier Tongues prior to their recent break ups). At the same time, the EGT is smaller in absolute scale by a factor of ten from these giant glacier tongues. Possibly the EGT is atypical in that it is protected from currents and waves by the Dellbridge Islands. Consequently, the relative scale of separated flow to that of the tongue is likely much larger for the EGT than for large glacier tongues or ice shelf fronts. However, vertical scales are greater for the big ice tongues so that vertical flows may be even stronger. If the flow is trying to get past a floating glacier and it is being forced down or up next to a wall then the higher the wall the greater the depth change and the greater the pressure effect on freezing point. Where the present data are of relevance to both the larger ice tongues, and indeed ice shelf fronts, is at the small scale. The EGT observations should be relevant wherever there is blockage of upper ocean flow.

The work here identified the complex flows that persist near glacier tongues. It demonstrated that the resulting mixing can be substantial. The data illustrate the small temporal

scales of variability in turbulence, the strong and fluctuating vertical flows, and the large dissipation rates and diffusivities possible next to the ice wall. Future work on the topic should seek to resolve spring-neap differences in mixing as well as relate the local mixing to the far-field transport in the Sound. Headland studies (Edwards et al., 2004) have demonstrated the effectiveness of spatial mapping of currents. However, such mapping is difficult in the presence of fast ice requiring underwater vehicle technology (e.g. Hayes and Morison, 2002; Doble et al., 2009). Modelling needs to progress at two scales. Over long timescales continual elevated mixing at a sub-grid location will influence circulation. Intermediate scales of regional modeling would elucidate this influence whilst finescale modeling would generate a valuable picture of where and how the mixing is generated. This modeling needs to be informed by velocity, scalar and turbulence measurements in a wide range of background stratification regimes.

**Acknowledgements.** The authors wish to thank Pat Langhorne, Andy Mahoney, Alex Gough, Robin Robertson, Inga Smith and Melissa Bowen for useful discussions. Brett Grant, Stéphane Popinet, David Plew, Brian Stait and Peter Gerring assisted with field work. Laurie Padman and two anonymous reviewers provided highly constructive criticism on the Ocean Science Discussion version of this manuscript. Satellite imagery is courtesy of NASA. Funding and support were provided by The New Zealand Royal Society administered Marsden Fund, Antarctica New Zealand (Events K131/K132) and the New Zealand Foundation for Research Science and Technology (Contract C01X0701). This paper is dedicated to the memory of Don Lewis.

Edited by: K. J. Heywood

## References

- Albrecht, N., Vennell, R., Williams, M., Stevens, C., Langhorne, P., Leonard, G., and Haskell, T.: Observation of sub-inertial internal tides in McMurdo Sound, Antarctica. *Geophys. Res. Lett.* 33, L24606, doi:10.1029/2006GL027377, 2006.
- Barry, J. P. and Dayton, P. K.: Current patterns in McMurdo Sound, Antarctica and their relationship to local biotic communities, *Polar Biol.*, 8, 367–376, doi:10.1007/BF00442028, 1988.
- Deacon, G. E. R.: The oceanographic observations of Scott's last expedition, *Polar Record*, 17, 391–419, 1975.
- Debenham, F.: The glacier tongues of McMurdo Sound, *Geogr. J.*, 131, 369–371, 1965.
- DeLisle, G., Chinn, T., Karlen, W., and Winters, P.: Radio echosounding of Erebus Glacier Tongue, New Zeal. *Antarc. Rec.*, 9, 15–30, 1989.
- Dempsey, D. E., Langhorne, P. J., Robinson, N. J., Williams, M. J. M., Haskell, T. G., and Frew, R. D.: Observation and modeling of platelet ice fabric in McMurdo Sound, Antarctica, *J. Geophys. Res.*, 115, C01007, doi:10.1029/2008JC005264, 2010.
- Dinniman, M. S., Klinck, J. M., and Smith Jr., W. O.: Influence of sea ice cover and icebergs on circulation and water mass formation in a numerical circulation model of the Ross Sea, Antarctica. *J. Geophys. Res.* 112, C11013, doi:10.1029/2006JC004036, 2007.
- Dmitrenko, I. A., Wegner, C., Kassens, H., Kirillov, S. A., Krumpfen, T., Heinemann, G., Helbig, A., Schröder, D., Hölemann, J. A., Klagge, T., Tyshko, K. P., and Busche, T.: Observations of supercooling and frazil ice formation in the Laptev Sea coastal polynya, *J. Geophys. Res.*, 115, C05015, doi:10.1029/2009JC005798, 2010.
- Doble, M. J., Forrest, A. L., Wadhams, P., and Laval, B. E.: Through-ice AUV deployment: Operational and technical experience from two seasons of Arctic fieldwork, *Cold Reg. Sci. Technol.*, 56, 90–97, 2009.
- Edwards, K., MacCready, P., Moum, J., Pawlak, G., Klymak, J., and Perlin, A.: Form drag and mixing due to tidal flow past a sharp point, *J. Phys. Oceanogr.*, 34, 1297–1312, 2004.
- Fer, I.: Scaling turbulent dissipation in an Arctic fjord, *Deep-Sea Res. PT II*, 53, 77–95, 2006.
- Frezzotti, M.: Ice front fluctuation, iceberg calving flux and mass balance of Victoria Land glaciers, *Antarct. Sci.*, 9, 61–73, 1997.
- Goring, D. G. and Pyne, A.: Observations of sea-level variability in Ross Sea, Antarctica, New Zeal., *J. Mar. Fresh.*, 37, 241–249, 2003.
- Hayes, D. R. and Morison, J. H.: Determining turbulent, vertical velocity, and fluxes of heat and salt with an autonomous underwater vehicle, *J. Atmos. Ocean. Technol.*, 19, 759–779, 2002.
- Hellmer, H. H.: Impact of Antarctic ice shelf basal melting on sea ice and deep ocean properties, *Geophys. Res. Lett.* 31, L10307, doi:10.1029/2004GL019506, 2004.
- Holdsworth, G.: Dynamics of Erebus Glacier tongue, *Ann. Glaciol.*, 3, 131–137, 1982.
- Jacobs, S. S., Huppert, H. E., Holdsworth, G., and Drewry, D. J.: Thermohaline steps induced by melting of the Erebus Glacier Tongue, *J. Geophys. Res.*, 86(C7), 6547–6555, 1981.
- Jeffries, M. O. and Weeks, W. F.: Structural characteristics and development of sea ice in the western Ross Sea, *Antarct. Sci.*, 5(1), 63–75, 1992.
- Legresy, B., Wendt, A., Tabacco, I., Remy, F., and Dietrich, R.: Influence of tides and tidal current on Mertz Glacier, Antarctica, *J. Glaciol.*, 50, 427–435, 2004.
- Leonard, G. H., Purdie, C. R., Langhorne, P. J., Haskell, T. G., Williams, M. J. M., and Frew, R. D.: Observations of platelet ice growth and oceanographic conditions during the winter of 2003 in McMurdo Sound, Antarctica, *J. Geophys. Res.*, 111, C04012, doi:10.1029/2005JC002952, 2006.
- Leonard, G. H., Purdie, C. R., Langhorne, P. J., Williams, M. J. M., and Haskell, T. G.: Ice crystals in the water column: the view from an Acoustic Doppler Current Profiler (ADCP), *IAHR Proceedings 20th IAHR International Symposium on Ice*, Helsinki, 2010.
- Lewis, E. L. and Perkin, R. G.: The winter oceanography of McMurdo Sound, Antarctica, *Antar. Res. S.*, 43, 145–165, 1985.
- Macoun, P. and Lueck, R. G.: Modelling the spatial response of the air-foil shear probe using different sized probes, *J. Atmos. Oceanic Technol.* 21, 284–297, 2004.
- Mahoney, A., Gough, A., Langhorne, P., Robinson, N., Stevens, C., Williams, M., and Haskell, T.: The seasonal arrival of ice shelf water in coastal Antarctica and its effect on sea ice growth, *J. Geophys. Res.*, in review, 2011.

- McPhee, M. G.: Air-ice-ocean-interaction: Turbulent Ocean Boundary Layer Exchange Processes, Springer, 215 pp., 2008.
- Olbers, D. and Hellmer, H.: A box model of circulation and melting in ice shelf caverns, *Ocean Dynam.*, 60, 141–153, doi:10.1007/s10236-009-0252-z, 2010.
- Osborn, T.: Estimates of the local rate of vertical diffusion from dissipation measurements, *J. Phys. Oceanogr.*, 10, 83–89, 1980.
- Pacanowski, R. C. and Philander, S. G. H.: Parameterization of vertical mixing in numerical models of tropical oceans, *J. Phys. Oceanogr.*, 11, 1443–1451, 1981.
- Prandke, H.: Microstructure sensors, in: *Marine Turbulence: Theories, Observations and Models*, edited by: Baumert, H. Z., Simpson, J. H., and Sundermann, J., Cambridge Univ. Press, 101–109, 2005.
- Reddy, T. E., Holland, D. M., and Arrigo, K. R.: Ross ice shelf cavity circulation, residence time, and melting: Results from a model of oceanic chlorofluorocarbons, *Cont. Shelf Res.*, doi:10.1016/j.csr.2010.01.007, 2010.
- Rignot, E., Koppes, M., and Velicogna, I.: Rapid submarine melting of the calving faces of West Greenland glaciers, *Nat. Geosci.*, 3, 187–191, doi:10.1038/ngeo765, 2010.
- Robinson, W. and Haskell, T. G.: Calving of Erebus Glacier tongue, *Nature* 346, 615–616, 1990.
- Robinson N. J.: The ocean boundary layer beneath Antarctic sea ice in the vicinity of an ice shelf, PhD Thesis, Univ. Otago, 2011.
- Robinson, N. J., Williams, M. J. M., Barrett, P. J., and Pyne, A. R.: Observations of flow and ice-ocean interaction beneath the McMurdo Ice Shelf, Antarctica, *J. Geophys. Res.*, 115, C03025, doi:10.1029/2008JC005255, 2010.
- Roget, E., Lozovatsky, I., Sanchez, X., and Figueroa, M.: Microstructure measurements in natural waters: Methodology and applications, *Progr. Oceanogr.*, 70, 126–148, 2006.
- Shih, L. H., Koseff, J. R., Ivey, G. N., and Ferziger, J. H.: Parameterization of turbulent fluxes and scales using homogeneous sheared stably stratified turbulence simulations, *J. Fluid Mech.*, 525, 193–214, 2005.
- Signell, R. P. and Geyer, W. R.: Transient eddy formation around headlands, *J. Geophys. Res.*, 96, 2561–2575, 1991.
- Sirevaag, A., McPhee, M. G., Morison, J. H., Shaw, W. J., and Stanton, T. P.: Wintertime mixed layer measurements at Maud Rise, Weddell Sea, *J. Geophys. Res.*, 115, C02009, doi:10.1029/2008JC005141, 2010.
- Smith I. J., Langhorne P. J., Haskell T. G., Trodahl H. J., Frew R., and Vennell M. R.: Platelet ice and the land-fast sea ice of McMurdo Sound, Antarctica, *Ann. Glaciol.*, 33, 21–27, 2001.
- Squire, V. A., Robinson, W. H., Meylan, M., and Haskell, T. G.: Observations of flexural waves on the Erebus Ice Tongue, McMurdo Sound, Antarctica, and nearby sea ice, *J. Glaciol.*, 40, 377–385, 1994.
- Sobey, I. J.: Oscillatory flows at intermediate Strouhal number in asymmetric channels, *J. Fluid Mech.*, 125, 359–373, 1982.
- Stevens, C. L., Williams, M. J. M., Robinson, N. J., Albrecht, N., and Haskell, T. G.: Observations of the stratified turbulent boundary-layer and platelet ice beneath McMurdo Sound Sea Ice, *Proc. Sixth International Symposium on Stratified Flows*, edited by: Ivey, G. N., Perth, Australia, 2006.
- Stevens, C. L., Robinson, N. J., Williams, M. J. M., and Haskell, T. G.: Observations of turbulence beneath sea ice in southern McMurdo Sound, Antarctica, *Ocean Sci.*, 5, 435–445, doi:10.5194/os-5-435-2009, 2009.
- Wolk, F., Yamazaki, H., Seuront, L., Lueck, R. G.: A new free-fall profiler for measuring biophysical microstructure, *J. Atmos. Oceanic Techn.*, 19, 780–793, 2002.
- Xing, J. and Davies, A. M.: The effects of large and small-scale topography upon internal waves and implications for tidally induced mixing in sill regions, *Ocean Dynam.*, 60, 1–25, 2010.
- Zaron, E. D. and Moum, J. N.: A new look at Richardson Number mixing schemes for equatorial ocean modeling, *J. Phys. Oceanogr.*, 39(10), 2652–2664, 2009.